Available online at www.sciencedirect.com

ScienceDirect

Geochimica et Cosmochimica Acta 329 (2022) 168–184

Geochimica et Cosmochimica Acta

www.elsevier.com/locate/gca

$CaCO_3$ dissolution in carbonate-poor shelf sands increases with ocean acidification and porewater residence time

Abby Lunstrum *, William Berelson

University of Southern California, 3651 Trousdale Pkwy, Los Angeles, CA 90089, United States

Received 30 August 2021; accepted in revised form 27 April 2022; Available online 5 May 2022

Abstract

Carbonate-poor sandy sediments comprise much of the shelf area, and—despite their low $CaCO_3$ content—contain a significant pool of $CaCO_3$ base available to neutralize ocean acid. Here, we conducted flow-through column experiments on permeable, carbonate-poor sand obtained from Catalina Island, CA, to quantify $CaCO_3$ dissolution across a range of current and future seawater conditions. Using ^{13}C isotope mass balance, we show that dissolution depends both on the $CaCO_3$ saturation state (Ω) of the inflowing seawater, as well as porewater residence time. At current ocean conditions ($\Omega_{aragonite} = 2.4$ and $\Omega_{calcite} = 3.7$ at our field site), dissolution was negligible for porewater residence times < 1.8 h, but increased thereafter, following sufficient production of CO_2 from aerobic respiration. As Ω of inlet water was lowered, simulating future ocean conditions, dissolution began earlier and rates increased. The response to acidification was similar to previously reported observations in carbonate-rich shelf environments, suggesting that carbonate-poor sediments have the potential to support enhanced dissolution in an acidifying ocean, given sufficient $CaCO_3$ substrate. With continued acidification projected to occur this century, these sediments could transition from a net source of acid to the overlying seawater (production of alkalinity to dissolved inorganic carbon, $\Delta Alk/\Delta DIC < 1$) to net source of buffering capacity ($\Delta Alk/\Delta DIC > 1$) when overlying seawater $\Omega_{aragonite}$ reaches 0.96 to 0.69 ($\Omega_{calcite} = 1.50$ and 1.07), depending on porewater residence time. In some areas with naturally acidic water, this threshold has already been reached.

Keywords: Ocean acidification; Carbonate dissolution; Permeable sediment; Ocean alkalinity

1. INTRODUCTION

The ocean has absorbed approximately one quarter of anthropogenic carbon dioxide (CO_2) emissions since preindustrial times, causing a decrease in global average seawater pH by 0.1 unit (Caldeira and Wickett, 2005; Friedlingstein et al., 2020). As CO_2 emissions continue, average global surface ocean pH is expected to fall by up to 0.5 unit by 2100 (Caldeira and Wickett, 2005). In a more acidic ocean, the dissolved inorganic carbon (DIC) pool is thermodynamically shifted away from carbonate ions (CO_3^{2-}), and the stability of calcium carbonate ($CaCO_3$) minerals decreases. The resulting dissolution of $CaCO_3$ releases alkalinity and consumes CO_2, constituting an important negative feedback on atmospheric CO_2 levels (as reviewed in Zeebe, 2012). While full sequestration of anthropogenic CO_2 is thought to require silicate weathering on the timescale of millions of years, $CaCO_3$ dissolution is relatively more important on shorter timescales (<10,000 y). In deep sea sediments, increased $CaCO_3$ dissolution in response to rising CO_2—termed "carbonate compensation"—depends on ocean circulation delivering high-CO_2 surface water to depth, and thus occurs on the > 1,000-y scale (Broecker and Peng, 1987). We are beginning to see signs of this

* Corresponding author.
E-mail addresses: lunstrum@usc.edu (A. Lunstrum), berelson@usc.edu (W. Berelson).

https://doi.org/10.1016/j.gca.2022.04.031
0016-7037/

process in the deep North Atlantic (Perez et al., 2018; Sulpis et al., 2018).

Sediments on the continental shelves are not typically considered in the discussion of carbonate compensation, as they are bathed in surface seawater with higher $CaCO_3$ saturation states (Zeebe and Westbroek, 2003). However, in theory, these sediments may respond quickly to acidifying surface seawater due to several factors, including: high concentrations of more soluble carbonate forms (aragonite and high-Mg calcite); high rates of organic matter (OM) deposition and respiration, which lower porewater pH; naturally acidic water from upwelling and/or terrestrial nutrient input; and, in the case of coarse-grained sediments, enhanced mineral-seawater interaction via porewater advection. Despite this potential, we currently have little understanding of how $CaCO_3$ in sediments on the continental shelf respond to ocean acidification.

The continental shelf comprises just 7% of global ocean area (Emery, 1968), but is disproportionately important in ocean carbon cycling. For example, 80% of marine organic matter (OM) burial and 90% of benthic respiration are estimated to occur in shelf sediments (Gattuso et al., 1998). Rapid mixing with deeper waters can then effectively shuttle respired CO_2 to depth, making the shelf area a more efficient CO_2 sink than surface waters of the open ocean (Tsunogai et al., 1999; Thomas et al., 2004; Cai, 2011). Furthermore, it is estimated that half of oceanic $CaCO_3$ is buried on the shelves, while the remaining half is distributed across the slopes and vast deep ocean (Milliman, 1993; Iglesias-Rodriguez et al., 2002). Despite this, $CaCO_3$ dynamics in shelf sediments remain poorly understood, and little has changed since Milliman and Droxler's (1996) assessment that "Of all the carbonate environments, we probably know the least about carbonate production, export, and accumulation on continental shelves.".

In studies focused on $CaCO_3$ cycling, the global shelf area is often divided into four environmental categories, including coral reefs, banks/bays, carbonate shelves, and carbonate-poor shelves. The latter two groups are easily divided as sediments are bimodal in terms of either high- or low-carbonate content (Milliman, 1993). While a comprehensive quantification of global shelf $CaCO_3$ content is beyond the scope of this study, it is clear from existing data that carbonate-poor sediments, composed primarily of detrital or relict silicates with minor amounts of biogenic $CaCO_3$, make up a significant fraction—by some estimates more than half—of the global shelf area (Milliman, 1993; Jenkins, 2021). Despite their large extent, they are not commonly studied for $CaCO_3$ dynamics, presumably due to their low $CaCO_3$ content (<1%) (Krumins et al., 2013). As a result, recent estimates of global $CaCO_3$ accumulation on the carbonate-poor shelf vary by two orders of magnitude (Iglesias-Rodriguez et al., 2002; O'Mara and Dunne, 2019). In contrast, there are many measurements of $CaCO_3$ dissolution in shallow-water, coral reef sands (Boucher et al., 1998; Yates and Halley, 2003; Yates and Halley, 2006; Andersson et al., 2007; Rao et al., 2012; Andersson and Gledhill, 2013; Cyronak et al., 2013b; Cyronak et al., 2013a; Eyre et al., 2014; Andersson, 2015; Cyronak and Eyre, 2016; Trnovsky et al., 2016; Fink et al., 2017; Eyre et al., 2018; Stoltenberg et al., 2020; Stoltenberg et al., 2021).

In addition to ecosystem type, shelf sediments can be further divided into fine-grained sediments, in which dissolved components in porewater move primarily through diffusion, and coarse-grained sediments (average grain size equal to or larger than very fine sand, 62.5 μm), in which porewater movement is driven by advective transport. In the latter, solute transport can exceed diffusive flows by several orders of magnitude (Precht and Huettel, 2004). Approximately half of the continental shelf is thought to be covered by coarse-grained sediments (Hayes, 1967; Hall, 2002). Porewater flow through these sands occurs on globally relevant scales, with the entire ocean volume filtering through sediments every 3,000 to 14,000 years (Riedl et al., 1972; Moore et al., 2008; Santos et al., 2012). This largescale movement of seawater acts as a "subtidal pump", stimulating biogeochemical processes via the delivery of oxygen (O_2) and OM to particle-attached microbes, fluctuating redox conditions, and removal of diagenetic byproducts (Riedl et al., 1972; Shum and Sundby, 1996; Rusch et al., 2006). As a result, benthic $CaCO_3$ dissolution can be higher under advective versus diffusive porewater conditions (Rao et al., 2012; Cyronak et al., 2013b; Cyronak et al., 2013a). Unfortunately, complex advection dynamics in permeable sands also makes quantifying processes and fluxes difficult; techniques commonly used in diffusion-dominated sediments (e.g., porewater profiles, core incubations, etc.) are not useful because they do not consider nor accurately reproduce in situ advection (Boudreau et al., 2001; Huettel et al., 2014). Instead, alternative techniques such as advective chambers, flumes, and flow-through columns are used in permeable sediments. Because these approaches are arguably more challenging to implement and/or interpret, measurements of $CaCO_3$ dissolution in permeable sediments are less common, and to our knowledge there are no direct measurements in carbonate-poor sands. Furthermore, few dissolution studies in sands exist outside of the tropics, although colder waters are already less saturated with respect to $CaCO_3$ minerals, and expected to be more sensitive to ocean acidification (Andersson et al., 2005).

This study attempts to fill this gap by measuring $CaCO_3$ dissolution in carbonate-poor sands collected from the California coast. We used flow-through columns with alkalinity, DIC, and C isotopic measurements to quantify $CaCO_3$ dissolution rates across a range of $CaCO_3$ saturation states predicted for the coming century. The flow-through column technique also allowed us to control porewater residence time and advection rate to assess the response to acidification in different advection conditions. In this way, we aim to improve our understanding of how sediments on the continental shelves respond to ongoing ocean acidification and other global changes (e.g., wave and current energy) that may affect porewater advection dynamics.

2. METHODS

2.1. Experimental setup

Flow-through sand column experiments, commonly referred to as flow-through reactor (FTR) experiments, were conducted in June-July 2018 and March-May 2019. Sand was collected from the low intertidal by surface grab samples from Fisherman's Cove on Catalina Island, off the coast of Los Angeles, CA, USA (33.4450289 N, 118.4838903 W (WGS84)). This sand was considered a reasonable representation of coarse-grained, detrital shelf sediments. Although seabed properties on the shelf are extremely varied, a global, quantitative analysis of grain size, OM content, etc. is beyond the scope of this paper (Jenkins, 2021). Following collection, sand was sieved through a 2-mm sieve to remove rocks and macrofauna. In all cases, very little, if any, material was retained by the sieve (i.e., gravel fraction was negligible). Sand was subsequently packed into columns, or stored under running seawater in the laboratory prior to packing (within 24 h of collection).

Columns were constructed from 5.7 cm inner diameter by 30 cm tall polycarbonate tubes, with each end enclosed by a mesh screen and rubber bungs connected to inlet/outlet tubing (Fig. 1). Sample ports were drilled into the columns at two intermediate heights, thus providing four total sampling ports at 0 (inlet), 8.5 (bottom), 18.5 (middle), and 26 cm (top) sand height. Columns were placed in a temperature-controlled room set to 19° C (June-July 2018) or 16° C (July 2018, and March-May 2019). The two selected temperatures were not tested as explicit experimental treatments, but instead represent spring (16° C) or annual (19° C) mean water temperatures at the research site.

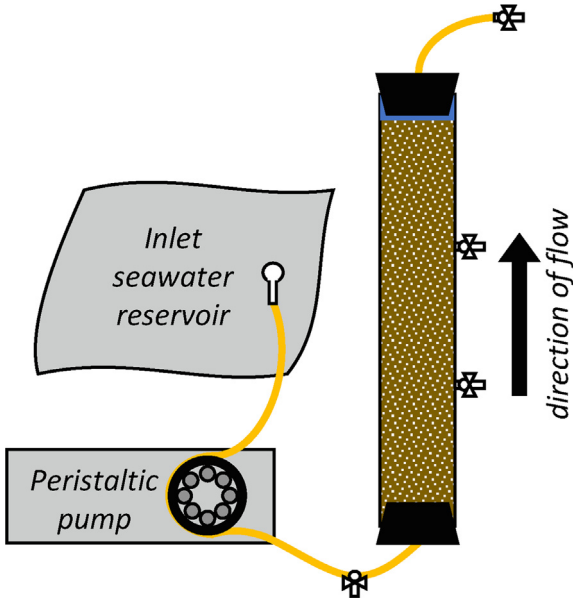

Fig. 1. Schematic of flow-through sand column. Water is peristaltically pumped from a gas-impermeable bag reservoir upward through the column. Sample ports are located below the column (0 cm sand height), at 8.5 cm, 18.5 cm, and above the column (26 cm sand height).

Packed columns were then connected via the lower (0 cm) port to approximately 50 cm of 1/8″ ID tubing (Tygon F-4040-A) connected via a peristaltic pump to a 5 or 10 L gas-impermeable, foil bag (Supel-Inert multi-layer foil with screwcap valve). Gas-proof bags were used instead of open bottles to eliminate the loss of CO_2 and thus maintain the carbonate saturation state (Ω) of the inlet seawater. Evacuated bags were pre-filled with 0.2 µm filtered seawater, also collected from Catalina Island. For some treatments, henceforth referred to as "acidified", inlet Ω was lowered by injecting HCl into the bags prior to the experiment. In this case, the bags were shaken for several hours prior to connecting to the columns to ensure thorough mixing of the acid. It should be noted that HCl lowers Ω by reducing alkalinity at a constant DIC, whereas in reality, ocean acidification increases DIC, but maintains alkalinity. Methodological studies have found no difference between these two manipulations on biological processes or $CaCO_3$ dissolution at a given Ω (Andersson and Mackenzie, 2012).

Water was peristaltically pumped from the bags, upwards through the columns at specified pump rates. Most experiments were run at 1 mL min^{-1}, but a subset was also run at 0.5 or 2 mL min^{-1} to test different advection rates and longer/shorter residence times. The 1 mL min^{-1} pump rate yielded porewater residence times of approximately 1.8, 3.6, and 5.4 h (for bottom, middle, and top ports, respectively), based on a measured porosity of 0.5. These nominal times are used throughout the discussion, but actual porewater residence times varied slightly for each column. Pump rates were verified by weighing outlet water after several hours, and adjusted as necessary to reach the target pump rate. By visual inspection during and after the experiment, there was no evidence of channeling or flow along the column sides. Breakthrough curve experiments using fluoride tracer also indicated no channeling, and the apparent dispersivity suggested an average variation in porewater residence time of approximately ± 10% (Supplemental Material).

Pump rates were selected to replicate realistic advection rates (also commonly referred to in the literature as "flushing rates"). Our advection rates ranged from 280 to 1130 L m^{-2} d^{-1}, similar to those measured in situ in medium-coarse sand by Reimers et al (2004) (300 to 1,300 L m^{-2} d^{-1}). In situ porewater advection measurements are scarce, but several studies have estimated *average* flushing rates that are slower than those used in our study, on the order of 100 L m^{-2} d^{-1} (Precht and Huettel, 2004; Santos et al., 2012; McGinnis et al., 2014). However, higher rates, up to 8,000 L m^{-2} d^{-1}, have been documented for high energy environments (McLachlan, 1989). A related, but distinct, metric for advection is porewater advective velocity. Our velocities—2.3 to 9.2 cm h^{-1}—were similar to those measured by Reimers et. al. for sediments deeper than 1 cm. Like advection rate, porewater velocities also vary widely depending on sediment depth and hydrodynamic forcing, and can range from < 1 to > 300 cm h^{-1}, although most hydrodynamic processes result in velocities of < 20 cm h^{-1} (Oberdorfer and Buddemeier, 1986;

Precht and Huettel, 2004). Thus, our advection rates were selected to represent a range of realistic conditions.

Pumping continued for at least 48 hours (equivalent to flushing the column volume > 8 times) prior to initial sample collection in order to remove respiratory byproducts accumulated during column preparation. During this time, the top outlet water was sampled and analyzed regularly to ensure that alkalinity and DIC were stable prior to taking samples for data analysis. Final samples were collected approximately 48–72 hours after pumping began for 1 and 2 mL min^{-1} experiments, and up to 146 hours after pumping began for the 0.5 mL min^{-1} experiments.

Samples were collected using glass syringes attached to one outlet port at a time, filling passively by pump pressure. Top port samples were collected first, then the lower ports collected in sequence (e.g., middle, then bottom) to avoid sampling stagnant porewater in the upper column following sampling at lower levels. For each sample, at least 40 mL water was collected for DIC and $\delta^{13}C$ (24 mL) and alkalinity (14 mL) analysis, as well as for O_2 for a subset of the 1 mL min^{-1} columns.

2.2. Isotope spike experiments

Two sets of column experiments were run with the addition of a small amount (50 mg) of either ^{13}C-labeled calcite (April 2019) or ^{13}C-labeled aragonite (May 2019) added to the sediment. These experiments served as a test to confirm the presence or absence of dissolution observed in the natural abundance experiments, and to constrain the Ω at which aragonite and calcite dissolution begins (Ω_{arag} and Ω_{calc}, respectively). (Dissolution *rates* were not calculated in these columns.) The ^{13}C-calcite (>99% ^{13}C) was purchased from Aldrich, and the ^{13}C-aragonite (100 ± 5% ^{13}C) was grown in our lab using a gel-diffusion method (Nickl and Henisch, 1969; Dong et al., 2019). Each ^{13}C spike was sieved to grain size fractions similar to the sand (between 0.05 mm and 2 mm), weighed, then thoroughly mixed into a bucket of drained sand, with just enough sand volume to fill the necessary columns. The mass of labeled carbonate added was approximately 0.5% of the total PIC present in the natural sand. This low spike addition was used to minimally alter the $CaCO_3$ content of the sand, yet provide a clear dissolution signal in $\delta^{13}C$. The amended sand had a ~ 50% increase in ^{13}F (the ratio of ^{13}C to total C content) compared to the natural sand, and the resulting $\delta^{13}C_{PIC}$ was 702‰ (±15) for the calcite experiment, and 457‰ (±164) for the aragonite experiment.

For both the calcite and aragonite spike experiments, four columns were incubated: two sets of paired spike/non-spike columns, one pair which was exposed to natural seawater (Ω_{arag} = 2.3 to 2.4), and the other pair which was exposed to acidified seawater (Ω_{arag} = 1.2 to 1.3). These four columns were incubated simultaneously to a) confirm no significant treatment effect of the isotope spike on alkalinity or DIC production, and b) to calculate dissolution of the spike using the isotopic difference between the paired spiked and control (non-spiked) columns.

2.3. Sample analysis – liquid phase

Dissolved O_2 concentrations were measured immediately upon sample collection. Measurements were taken by microsensor electrode (A/V Unisense) in 2018, or by optode (NeoFox, Ocean Optics) in 2019, in both cases standardizing between air-saturated and anoxic (N_2-purged) seawater. Error on O_2 measurements was assumed to be 5%.

For alkalinity, DIC and $\delta^{13}C$, water samples were filtered (0.45 μm pore size), refrigerated and analyzed within one week of collection. Alkalinity samples were collected in 15 mL Falcon tubes, and measured by open-system Gran titration on a custom-built instrument consisting of an electrode connected to a pH meter (Metrohm Ecotrode and Mettler Toledo SevenCompact, respectively) and electronic titrator (Metrohm 876 Dosimat Plus). Weighed samples were equilibrated to 21C, stirred, and aerated during titration with 0.05–0.1 M HCl, as controlled by a custom MATLAB script that adds acid in 0.01 mL increments and measures pH in 20 s intervals. After 12 time points, the alkalinity endpoint was determined using a nonlinear least-squares approach. A standard reference (Dickson seawater) was run at the beginning of each analytical run to ensure consistency. Long-term alkalinity precision (standard deviation) for this analysis is about 4 μeq kg^{-1} over several months.

Aliquots for DIC and $\delta^{13}C$ analysis were collected in duplicate by injecting 7 mL sample into pre-evacuated 12 mL exetainer vials (Labco). Samples were transferred directly from the glass syringe, through a filter, into the vials, thereby avoiding DIC loss from outgassing. Samples were then measured with a cavity ringdown spectrometer (CRDS; Picarro Model G-2131) coupled to a Picarro Liaison interface and a modified Automate autosampler. Approximately 3 mL of 10% H_3PO_4 was added to each sample, and the CO_2 carried with N_2 carrier gas through a Nafion desolvating line, to the CRDS. Standard references (OPT calcite calibrated against measurements at the UC Davis Stable Isotope Lab and Dickson seawater) were included in each analytical run. Both DIC and $\delta^{13}C$ were normalized to multiple standards and corrected for blanks, water content, and machine drift, as appropriate. The precision (standard deviation) for this method was < 12 μmol kg^{-1} for DIC and < 0.15‰ for $\delta^{13}C$.

2.4. Sample analysis – solid phase

Sand used in the incubations was analyzed for solid phase parameters, including grain size, porosity, percent total particulate C, and particulate inorganic C (TC and PIC, respectively), as well as the $\delta^{13}C$ of TC and PIC. For a subset of incubations, percent particulate organic C (POC) and its associated $\delta^{13}C$ were also measured. %TC and $\delta^{13}C_{TC}$ were analyzed on 50 mg sand aliquots which were dried, ground, and packed in 6x10 mm tin capsules, then combusted on a Costech ECS 4010 Elemental Analyzer, coupled to the CRDS. %PIC and $\delta^{13}C_{PIC}$ were analyzed by weighing 150 mg aliquots into 12 mL exetainer

vials, which were subsequently evacuated, injected with 5 mL 10% H_3PO_4, vortexed to convert PIC to CO_2 gas, then run through the CRDS. For %POC and $\delta^{13}C_{POC}$, dried and ground aliquots were weighed into 6x10 mm silver capsules, then acidified with H_3PO_4 until bubbling ceased. After drying, the silver capsules were packed into larger (9x10mm) tins, and analyzed on the Elemental Analyzer-CRDS system. For experiments where POC was not measured directly, %POC was calculated as the difference between %TC and %PIC, and $\delta^{13}C_{POC}$ calculated from the PIC, TC, and OC isotope mass balance. This approach was confirmed to be reasonable by comparing measured and calculated POC and $\delta^{13}C_{POC}$ values for experiments with both data available: OC differed by < 0.01 %C and $\delta^{13}C_{OC}$ by < 0.5‰.

Carbonate mineralogy was determined both by Raman spectroscopy and x-ray diffraction (XRD) at the Natural History Museum of Los Angeles County. Sand porosity was measured by mass difference between wet and dry samples (60C oven until constant weight), assuming a mineral density of 2.6 g cm^{-3} and correcting for seawater salt content. The sand grain size distribution was measured by wet, then dry sifting with metal sieves ranging in mesh size from 2 mm to 62.5 μm.

2.5. Calculations

Alkalinity and DIC data were used to calculate Ω_{arag} and Ω_{calc} using either the CO2SYS Excel macro (v 2.05) or Matlab code (v 1.1) (Lewis and Wallace, 1998; van Heuven et al., 2011), with options set as: total pH scale, K_{HSO4} from Dickson (1990), and CO_2 constants from Mehrbach et al (1973), refit by Dickson and Millero (1987). Uncertainties were calculated using analytical errors and default errors for thermodynamic constants defined in Orr et al. (2018).

Production (or consumption) of DIC, alkalinity, and O_2 was assessed as the difference between inlet and outlet concentrations at each port (for example for DIC):

$$DIC_{added} = DIC_{out} - DIC_{in} \quad (1)$$

Where DIC_{out} and DIC_{in} are the concentrations of DIC measured at each outlet or the inlet, respectively (μmol kg^{-1}). Areal production (or consumption) rates were then calculated at each outlet port, on a time-normalized basis as (for example for DIC):

$$Production\ rate = (DIC_{added})(1.025)(Q)/(A) \quad (2)$$

Where 1.025 kg L^{-1} considers the density of seawater; Q is the flow rate of the experiments (in L h^{-1}); and A is the cross-sectional area of the sand column (0.0026 m^2). A similar procedure was followed to calculate alkalinity production (Alk_{added}) and O_2 consumption (using Eq. (1)) and their respective areal production rates (using Eq. (2)).

$CaCO_3$ dissolution was calculated based on the isotope mass balance difference between inlet and outlet water, per the following equations:

$$(DIC_{added})(\delta^{13}C_{added}) = (DIC_{out})(\delta^{13}C_{out}) - (DIC_{in})(\delta^{13}C_{in}) \quad (3)$$

$$(DIC_{added})(\delta^{13}C_{added}) = (DIC_{PIC})(\delta^{13}C_{PIC}) + (DIC_{OM})(\delta^{13}C_{OM}) \quad (4)$$

Where $\delta^{13}C_{added}$ is the mean value of seawater $\delta^{13}C$ added between the inlet and outlet port, and DIC_{PIC} and DIC_{OM} refer to DIC production from PIC and OM, respectively. The only two unknowns—DIC_{PIC} and DIC_{OM}—can

Table 1
Measured alkalinity, DIC and O_2 production or consumption; calculated DIC added from OM respiration (DIC_{OM}); and calculated PIC dissolution (DIC_{PIC}) from a representative sample of columns (those for which O_2 was measured). DIC_{OM} values were calculated using O_2 data and a respiration quotient of 1.1. For comparison, DIC_{PIC} values were calculated with two different methods, using either the ^{13}C budget, or the DIC budget (DIC_{added} minus DIC_{OM}). Both methods yield DIC_{PIC} within analytical error for most columns. DIC_{PIC} calculated using the ^{13}C budget are used throughout the text. Approximate errors (standard deviation) are as shown for calculated values; 7 μmol kg^{-1} for measured Alk_{added}; 17 μmol kg^{-1} for measured DIC_{added}; and 12 μmol kg^{-1} for O_2 consumed.

Inlet Ω_{arag}	Porewater residence time (h)	Alk_{added} (μmol kg^{-1})	DIC_{added} (μmol kg^{-1})	O_2 consumed (μmol kg^{-1})	DIC_{OM} (μmol kg^{-1})	DIC_{PIC} from ^{13}C budget (μmol kg^{-1})	DIC_{PIC} from DIC budget (μmol kg^{-1})
0.12	*1.8*	605	400	−120	133 (±10)	326 (±52)	268 (±53)
	3.6	827	493	−160	176 (±10)	347 (±39)	317 (±40)
	5.4	920	574	−170	187 (±10)	397 (±38)	387 (±40)
1.04	*1.8*	61	130	−110	121 (±9)	12 (±3)	10 (±10)
	3.6	250	224	−152	167 (±9)	58 (±9)	58 (±13)
	5.4	332	271	−151	166 (±9)	101 (±15)	105 (±17)
1.29	*1.8*	80	189	−148	162 (±14)	22 (±4)	27 (±14)
	3.6	211	326	−225	248 (±13)	96 (±11)	78 (±17)
	5.4	273	337	−236	259 (±13)	84 (±9)	78 (±16)
2.42	*1.8*	9	121	−132	146 (±10)	−17 (±5)	−25 (±11)
	3.6	50	195	−152	167 (±10)	22 (±4)	28 (±10)
	5.4	141	263	−156	171 (±10)	65 (±9)	91 (±13)
2.43	*1.8*	−24	138	−148	162 (±14)	−33 (±7)	−24 (±16)
	3.6	25	231	−227	249 (±13)	6 (±1)	−18 (±13)
	5.4	73	249	−233	257 (±13)	3 (±0)	−8 (±13)

be solved for using Eqs. (1), (3), and (4), and the reasonable assumption that added DIC originates only from PIC and OM. For comparison and validation of the isotope budget approach, DIC_{PIC} was also calculated independently for a subset of columns (those for which O_2 was measured) using the DIC budget, as DIC_{added} minus DIC_{OM} derived from O_2 measurements (Table 1). For this calculation, DIC_{OM} production was calculated using O_2 consumption and a respiration quotient ($-O_2$ consumed:DIC_{OM} respired) of 1.1 (Moreno et al., 2020). Errors for all derived values were calculated by propagation of average analytical errors.

For the ^{13}C-spike experiments, $CaCO_3$ dissolution was not explicitly calculated, as the kinetics of biogenic and abiotic $CaCO_3$ dissolution can vary (Subhas et al., 2018). Rather, any increase in $\delta^{13}C$ in the spiked column samples was taken as evidence of spike dissolution. This is presented hereafter as $\Delta\delta^{13}C$, the difference between the $\delta^{13}C$ of the spike ($\delta^{13}C_{out\_spike}$) and control ($\delta^{13}C_{out\_control}$) column outlet water. This approach assumes identical $\delta^{13}C$ for the inlet water of both columns, which was confirmed within analytical error. Because a small amount of spike dissolution results in a large increase in $\delta^{13}C$, the spiked experiments provide a highly sensitive method for confirming dissolution of the different $CaCO_3$ crystal forms under different inlet Ω values.

3. RESULTS

3.1. Sediment characterization

Porosity averaged 0.51 (±0.02), and grain size was dominated by medium-coarse sand (grain size distribution: 19%, 36%, 38%, 7%, and 0% for > 1 mm, 0.5 to 1 mm, 0.25 to 0.5 mm, 0.06 to 0.25 mm, <0.06 mm, respectively). Carbon content was consistently low across collection dates: TC averaged 0.25% (±0.01%), with PIC 0.10% (±0.01%) and POC 0.14% (±0.01%). $\delta^{13}C$ values varied slightly across experimental dates, with $\delta^{13}C_{TC}$ ranging from −11.2 to −14.5‰; $\delta^{13}C_{PIC}$ from −0.9 to −4.1‰; and $\delta^{13}C_{OC}$ from −19.5 to −20.1‰. Given the small PIC content, quantitative mineralogical analysis was not possible. Raman spectroscopy and XRD both confirmed the presence of calcite

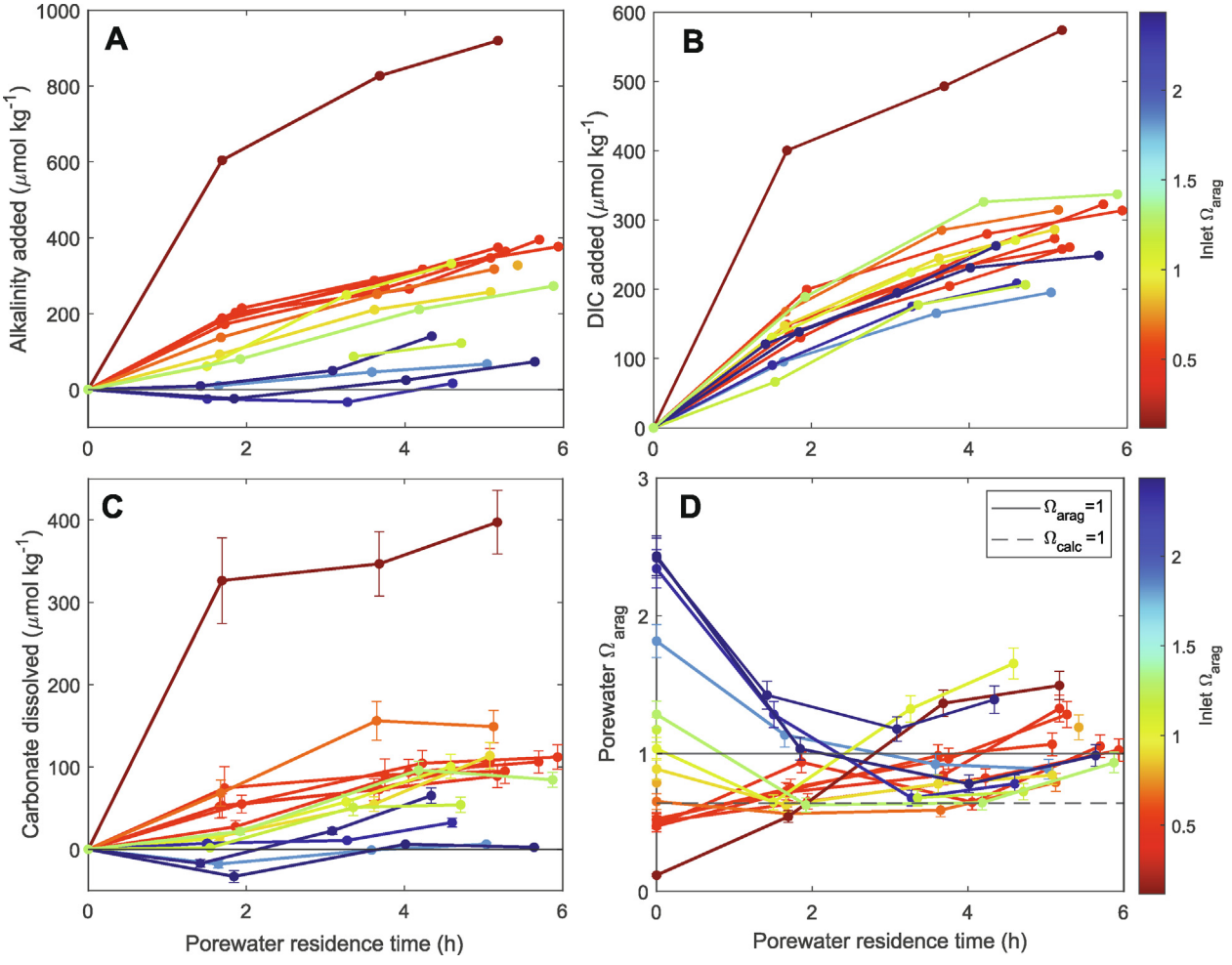

Fig. 2. Alkalinity added (A), DIC added (B), $CaCO_3$ dissolution determined by ^{13}C isotope budget (C), and porewater Ω (D) with respect to porewater residence time. Each line represents a single column experiment at 1 ml min^{-1} advection rate, with line color indicating $\Omega_{aragonite}$ of the inlet seawater. Analytical errors (SD) are 5.6 μmol m^{-2} h^{-1} for alkalinity added; 17 μmol m^{-2} h^{-1} for DIC added; and as shown for $CaCO_3$ dissolved and Ω.

and aragonite, but the counts of each were too low for statistically significant quantification.

3.2. Consumption or production of alkalinity, DIC, and O_2, and $CaCO_3$ dissolution

Alkalinity was generated in all columns, and there was a clear pattern of higher cumulative alkalinity production at lower inlet Ω (Fig. 2A; Table S1). In the high Ω (non-acidified) columns, alkalinity production was negligible prior to 1.8 h, but net positive by the end of the experiment at 5.4 h. In the acidified columns (inlet $\Omega_{arag} < 2$) however, alkalinity production was positive over all sampling points. The timing of peak alkalinity production also varied by inlet Ω: columns with inlet $\Omega_{arag} < 1$ typically had peak alkalinity production (as indicated by the slope of lines in Fig. 2A) between 0 and 1.8 h, whereas those with $\Omega_{arag} > 1$ had peak production after 1.8 h.

Total DIC production was not well correlated with inlet Ω, apart from generally lower production in the unacidified columns and very high DIC production in the most acidic column (inlet $\Omega_{arag} = 0.11$) (Fig. 2B; Table S2). This reflected the combined variability in DIC_{PIC} (DIC from $CaCO_3$ dissolution) at a given Ω (as in Fig. 2C) and DIC_{OM} between columns. Rates of DIC_{OM} production likely varied in part due to variable inlet O_2; in the ten columns for which inlet O_2 was measured, inlet O_2 was typically > 215 μmol kg^{-1}, although three had lower O_2, between 161–175 μmol kg^{-1}, suggesting incomplete air equilibration prior to initiating some experiments (Table S3). However, this variability in inlet O_2 was small in comparison to the range of inlet Ω's tested, and did not have a systematic effect on $CaCO_3$ dissolution with respect to inlet Ω. O_2 consumption was highest during the first 1.8 h, after which time porewater became hypoxic (<60 μM). While O_2 consumption rates slowed over time, O_2 concentrations continued to decrease, with a small amount remaining after 3.6 h, and most columns reaching < 5% saturation by 5.4 h.

$CaCO_3$ dissolution calculated with the ^{13}C isotope budget (Eqs. (1), (3), and (4)) and with the DIC budget (DIC_{added} minus DIC_{OM} calculated from O_2 consumption) were within analytical error for most measurements (Table 1). Henceforth, dissolution will refer to values calculated with the ^{13}C isotope budget unless otherwise noted. $CaCO_3$ dissolution was observed in all columns, and, like alkalinity production, was inversely correlated with inlet Ω (Fig. 2C). Dissolution rates also varied over porewater residence time, with different patterns for low- and high-Ω columns: in the high-Ω (unacidified) columns, $CaCO_3$ dissolution was negative (i.e., net precipitation) or near 0 at porewater residence times < 1.8 h, but positive thereafter. In the acidified columns, however, $CaCO_3$ dissolution was already positive by the first sampling point at 1.8 h. Most of the acidified columns had peak dissolution rates between 0–1.8 h or 1.8–3.6 h, and decreased thereafter, while some of the unacidified cores had increasing dissolution rates through the end of the experiment. Columns treated with different pumping rates had similar $CaCO_3$ dissolution rates when normalized for porewater residence time, indicating no clear effect of advection rate across the range tested (Fig. 3).

Porewater Ω changed over time in all columns (Fig. 2D). For columns with inlet water $\Omega_{arag} > 0.65$ ($\Omega_{calc} > 1$), Ω initially fell before rising again after 1.8 h. Most of these columns fell to a minimum porewater Ω between calcite and aragonite saturation. For columns with inlet $\Omega_{arag} < 0.65$, Ω steadily increased over the entire experiment. Regardless of initial Ω, all columns had stable or increasing Ω by the end of the experiment, with many columns reaching $\Omega_{arag} > 1$ by the last sampling point.

The relationship between inlet seawater Ω and cumulative $CaCO_3$ dissolution was approximated well by linear models for all three porewater residence times (1.8-, 3.6-, and 5.4-h, respectively; $r^2 = 0.711$, 0.619, and 0.547; $p < 0.001$, <0.001, and 0.002; Fig. 4). All three regressions had similar slopes. Although mechanistic studies of dissolution kinetics have shown non-linear dissolution rates with

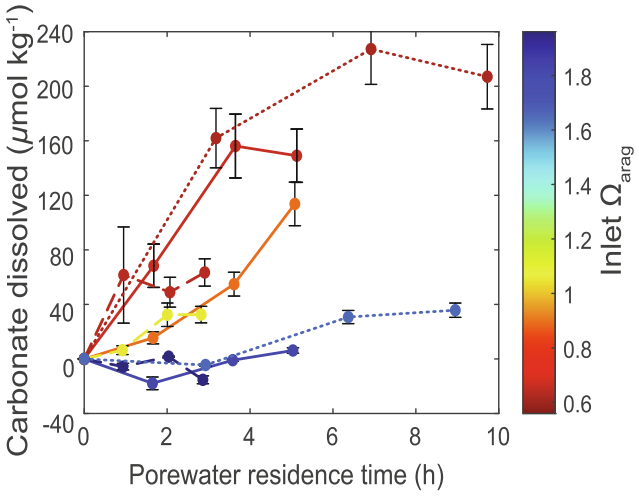

Fig. 3. $CaCO_3$ dissolution with respect to porewater residence time for three different advection rates. Dashed line: 2 ml min^{-1}; solid line: 1 ml min^{-1}; dotted line: 0.5 ml min^{-1}.

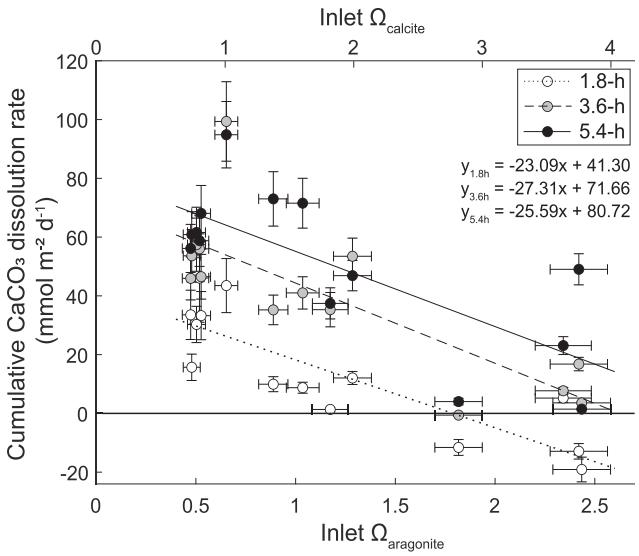

Fig. 4. $CaCO_3$ dissolution rates, normalized to sediment surface area, as a function of Ω_{inlet}. Linear relationships are shown for all three residence times: $r^2 = 0.711$, 0.619, and 0.547; $p < 0.001$, <0.001, and 0.002, for 1.8-, 3.6-, and 5.4-h porewater residence time, respectively. All data are from 1 ml min^{-1} advection rate experiments. (Figure and linear fit exclude data for the inlet $\Omega_{aragonite} = 0.1$ experiment.).

respect to Ω for single $CaCO_3$ morphotypes in undersaturated water, we assume our sand contains a mixture of morphotypes, and thus use a linear model as an approximation (Subhas et al., 2017; Naviaux et al., 2019).

Alkalinity and DIC production for the columns with ^{13}C-labeled $CaCO_3$ were the same (within error) as the unspiked column for all sampling points, indicating that the small ^{13}C spike did not affect bulk $CaCO_3$ dissolution or respiration rates. However, $\delta^{13}C$ increased in the spiked columns relative to the controls (i.e., $\Delta\delta^{13}C > 0$), indicating dissolution of the ^{13}C-spiked mineral (Fig. 5). In the high-Ω (non-acidified) seawater columns, $\Delta\delta^{13}C$ was significantly, yet only slightly > 0 (aragonite), or insignificant (calcite) at 1.8 h, indicating little or no dissolution of the spike under short residence time conditions (Fig. 5A, and 5B, respectively). However, after 1.8 h, both high-Ω experiments had $\Delta\delta^{13}C > 0$, suggesting dissolution of both $CaCO_3$ species. In the acidified columns, $\Delta\delta^{13}C$ was positive by the first sampling point at 1.8 h for both mineral species, indicating a more rapid onset of dissolution than in the high-Ω conditions.

4. DISCUSSION

4.1. Methodological considerations

Studies of $CaCO_3$ dissolution in permeable sediments typically use the Alkalinity Anomaly Technique, which assumes that dissolution is the sole alkalinity source during an incubation (i.e., total alkalinity = $CaCO_3$ dissolution * 2). This assumption has been shown to be reasonable for carbonate-rich coral reef sands where anaerobic respiration is minimal (Chisholm and Gattuso, 1991; Rao et al., 2012). However, in our natural abundance (i.e., non-^{13}C-spiked) experiments, comparing the dissolution rates calculated by ^{13}C isotope mass balance and total alkalinity production suggests that sources other than dissolution account for a variable but significant fraction of total alkalinity, averaging at least 20% (Fig. 6). The estimated global average for non-carbonate alkalinity on the carbonate-poor shelf is even higher, at 58% (Krumins et al., 2013). In these cases, the ^{13}C method is a better option than the Alkalinity Anomaly Technique, as it is not affected by non-carbonate alkalinity.

Two additional considerations of the ^{13}C isotope budget method merit discussion. First, fermentation in temporarily anoxic sands can produce DIC with extremely positive $\delta^{13}C$ (> +20 ‰) (Bourke et al., 2017; Kessler et al., 2019; Kessler et al., 2020). Addition of such positive $\delta^{13}C$ would increase $\delta^{13}C_{added}$, overestimating $CaCO_3$ dissolution in a two-endmember isotope mixing model (since $CaCO_3$ is the more positive $\delta^{13}C$ endmember, relative to OM). In our experiments, however, all data points except one—including the least oxic water between the top port and outlet—had $\delta^{13}C_{added}$ values between the OM and PIC endmembers. We thus assume that fermentation does not interfere significantly with our two-endmember analysis. The second potential issue with the ^{13}C method is $CaCO_3$ precipitation. The two-endmember mixing model ignores precipitation (Eq. (4)), because the system is underconstrained for a potential third endmember. Precipitation cannot simply be considered "negative dissolution" because the $\delta^{13}C$ of porewater (which precipitates) may be distinct from that of PIC (which dissolves); however, because the $\delta^{13}C$ of porewater (typically around + 1‰) is more similar to that of PIC (-1 to −3‰) than OM (-20‰), precipitation is *approximately* equal to "negative dissolution". Thus, calculated $CaCO_3$ dissolution rates are approximately equal to net dissolution. These considerations, and the fact that $CaCO_3$ dissolution calculated using two different approaches—by isotope mass balance and by the DIC budget)—lead us to conclude that our isotope mass balance-

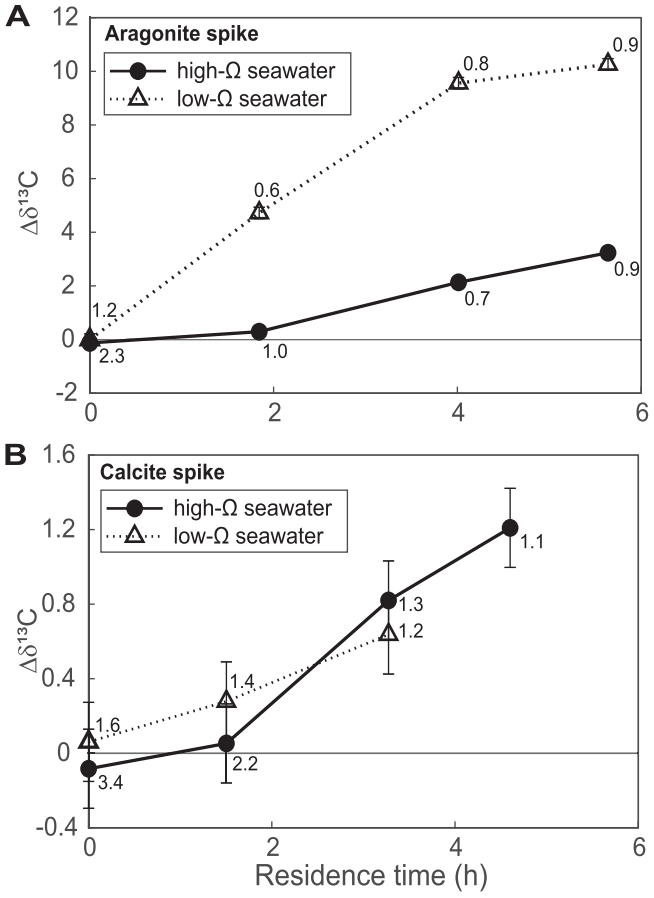

Fig. 5. Evolution of $\delta^{13}C$ for the ^{13}C-aragonite (A) and ^{13}C-calcite (B) spike experiments. The y axis ($\Delta\delta^{13}C$) represents the difference in outlet water $\delta^{13}C$ of the paired ^{13}C-spiked and natural cores: a positive value indicates higher outlet $\delta^{13}C$ in the spiked cores, resulting from dissolution of the spike $Ca^{13}CO_3$. Numbers next to each point indicate porewater Ω for the respective mineral species at each sampling point. "High-Ω" treatments use unaltered seawater, whereas "low-Ω" treatments are acidified to near-future conditions. Error (SD) are shown for $\Delta\delta^{13}C$ (smaller than point size for aragonite), and approximately 0.1 for Ω.

derived dissolution rates are reasonable estimates of net dissolution (Table 1).

Other methodological considerations relate to how our experimental setup differs from in situ conditions, including: no photosynthetically active radiation (PAR; i.e., dark-only conditions), constant temperature, use of filtered water, repacked sand, and constant advection rate and temperature. In shallow environments, photosynthesis at the sediment surface can increase Ω and depress $CaCO_3$ dissolution (Yates and Halley, 2006; Rao et al., 2012; Cyronak et al., 2013b; Fink et al., 2017; Lantz et al., 2017a). Our data should thus be considered representative of dissolution from deeper sites beyond the reach of PAR and/or nighttime rates. Approximately two-thirds of the shelf area is below the effective photic zone, so dark rates are applicable to a significant area (Gattuso et al., 2006). Similarly, our choice of a constant, annual average temperature represents only a subset of in situ climate conditions. Both OM respiration rates and $CaCO_3$ kinetics vary with temperature, and recent studies in coral reef sands have shown a clear effect of temperature on benthic $CaCO_3$ dissolution (Trnovsky et al., 2016; Stoltenberg et al., 2020). Future studies should assess this effect in carbonate-poor sands.

Because our primary variable of interest was Ω, we used filtered seawater to maintain a stable inlet Ω. Some studies have shown that particulate OM (POM) can be respired quickly in permeable sands, contributing to benthic metabolism and enhanced $CaCO_3$ dissolution (Bühring et al., 2006; Franke et al., 2006; Lantz et al., 2017b; Lantz et al., 2020). However, other studies have shown that POM may be highly recalcitrant (Megens et al., 2001), and may not have a significant effect on benthic O_2 demand in sands (Wild et al., 2005). The suspended POC concentration in seawater along the California coast is typically 10 to 20 μM (Amos et al., 2019). If 10 μM of POC were completely respired in the sand column, the porewater Ω_{arag} would drop by a maximum of 0.09, which could slightly increase $CaCO_3$ dissolution rates. Thus, at worst, the use of filtered water in our experiment leads to conservative $CaCO_3$ dissolution rates; and at best, it has no impact. Our columns also used repacked sand, which may have altered the in situ geochemical and/or biological profile.

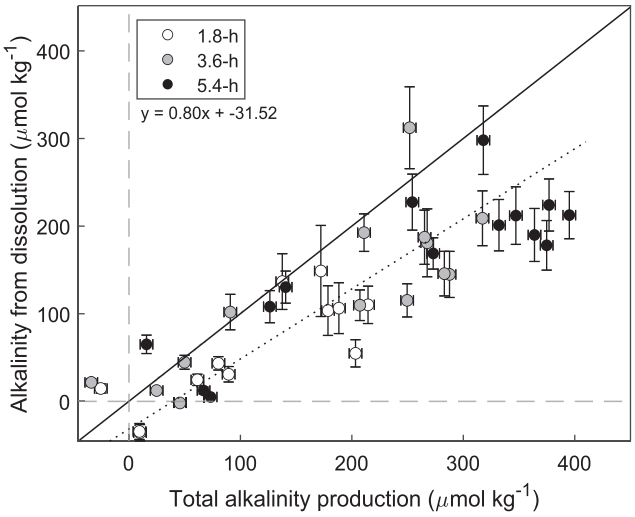

Fig. 6. Alkalinity from $CaCO_3$ dissolution (calculated from ^{13}C mass balance) versus total alkalinity production. The regression slope (dotted line) suggests alkalinity produced by $CaCO_3$ dissolution accounts for on average 80% of total alkalinity. Other alkalinity sources include anaerobic OM respiration (see text). Solid line is 1:1, shown for reference.

We believe this effect to be minor, however, since the sand was collected from a high-energy intertidal zone, where microbial gradients in surface sediment are unlikely.

Finally, our flow-through column setup uses constant, unidirectional advection. In reality, porewater advection in continental shelf sediments varies drastically over episodic, diurnal, and seasonal timescales, driven by dynamic processes like bio-irrigation, tidal and wave pumping, ripple migration, and flow interaction with sediment topography (Precht and Huettel, 2003; Santos et al., 2012; Huettel et al., 2014). Thus, a constant advection rate may not accurately reflect the dynamic redox and pH conditions experienced by much of the shelf sediment volume, especially at the sediment–water interface. However, because we have framed our analysis in terms of porewater residence time, we presume that our results can be applied to future in situ analyses of varying advection regimes.

4.2. $CaCO_3$ dissolution rates vary with porewater residence time

Our results clearly show that decreased Ω results in increased $CaCO_3$ dissolution; however, the magnitude of this effect depends on porewater residence time (Fig. 4). Thus, we first discuss the progression of porewater carbonate chemistry over time before discussing overall effects related to inlet seawater Ω.

Dissolution rates progressed differently over time, according to inlet Ω. In the columns exposed to the highest Ω (unacidified) seawater, dissolution was initially negative or near-0 and then increased toward peak rates near the end of the experiment (Fig. 2C). In contrast, dissolution in the acidified columns peaked earlier, at or prior to 1.8 h for the most acidified ($\Omega_{arag} < 0.6$) columns. After this initial period of differentiation, however, similar dissolution rates prevailed across all columns as porewater Ω's converged toward more similar values (Fig. 2D). The consequence of this effect can be seen in Fig. 4, wherein the dissolution vs. Ω slope is established by 1.8 h, and additional porewater residence time simply adds a constant dissolution rate to all columns, resulting in an unchanged slope, but higher x- and y-intercepts.

This time-dependence was driven by two different processes: (1) in low-Ω columns, a pulse of dissolution occurred as an immediate result of inlet undersaturation; and (2) in high-Ω columns, dissolution was delayed until OM respiration sufficiently lowered porewater Ω. These phenomena are illustrated by the Alkalinity:DIC vectors in Fig. 7. For the first 1.8 h porewater residence time, the low-Ω column vectors approach a slope of 1.8, indicating substantial $CaCO_3$ dissolution (since each mol of $CaCO_3$ dissolved produces two mol of alkalinity and one mol DIC). In contrast, the high-Ω columns initially have a slope near −0.2, indicative of aerobic OM respiration (since alkalinity is slightly decreased by the respiratory regeneration of alkalinity-consuming nutrients) and little $CaCO_3$ dissolution (Wolf-Gladrow et al., 2007). It is not until after 1.8 h that the high-Ω vectors turn toward the dissolution trajectory. After 3.6 h, all columns have relatively similar trajectories with positive alkalinity production, as they have more similar porewater Ω, and aerobic respiration is consistently low due to hypoxic porewater.

Benthic $CaCO_3$ dissolution is often considered to be tightly coupled with OM respiration via "metabolic dissolution", following the net reaction:

$$CaCO_3 + CH_2O + O_2 \rightarrow Ca^{2+} + 2HCO_3^- \quad (5)$$

(Emerson and Bender, 1981; Morse, 1985; Jahnke et al., 1994). However, our high-Ω columns show a lag between OM respiration and the onset of $CaCO_3$ dissolution in oversaturated water. Thus, the two processes are not necessarily coupled over short porewater residence times.

This decoupling between OM respiration and $CaCO_3$ dissolution has been described by Andersson (2015), in that

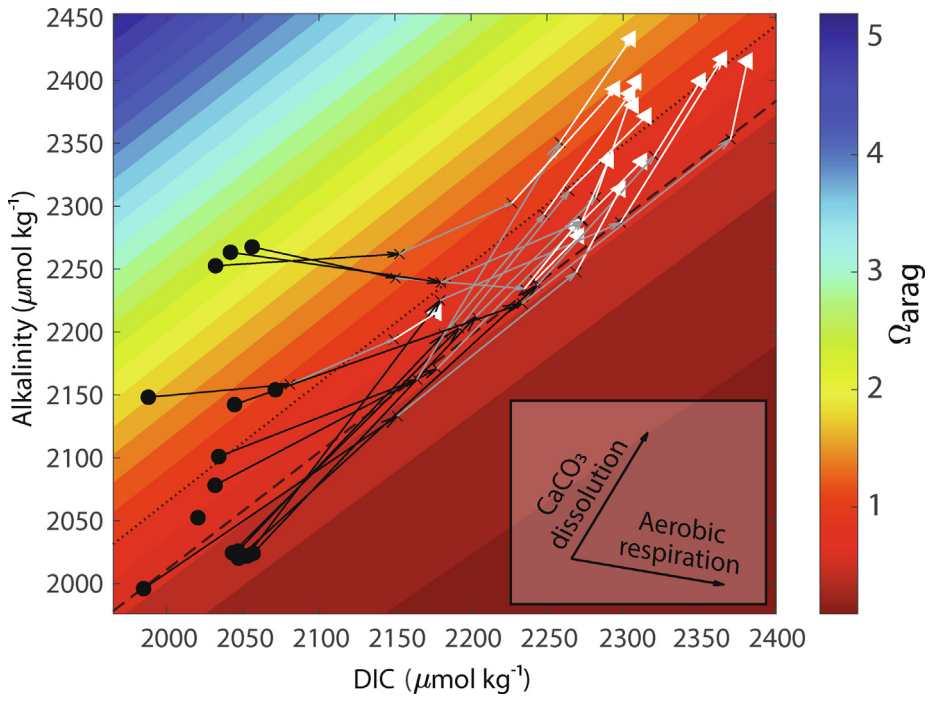

Fig. 7. Vectors for 1 mL min^{-1} experiments in alkalinity-DIC space, with background color indicating $\Omega_{aragonite}$. Each column is represented by three vectors, with porewater residence time represented by vector color: 0–1.8 h (black), 1.8–3.6 h (gray), and 3.6–5.4 h (white). Black circles represent inlet water, white triangles outlet water, and x's for intermediate points. Calcite and aragonite $\Omega = 1$ lines are shown as dashed and dotted lines, respectively. The key shows the vector direction (with arbitrary magnitude) for $CaCO_3$ dissolution and aerobic OM respiration. Approximate uncertainties are 5.6 μmol kg^{-1} for alkalinity, and 17 μmol kg^{-1} for DIC. (Figure excludes data for the $\Omega_{aragonite} = 0.1$ experiment.).

coupled metabolic dissolution occurs only after a critical Ω threshold is reached. In our experiments, we do not have the resolution to see the exact porewater Ω at which dissolution initiates, however the regression for our shortest (1.8-h) porewater residence time indicates net dissolution starts to occur at inlet $\Omega_{arag} = 1.75$ (Fig. 4). This dissolution threshold likely depends on $CaCO_3$ mineralogy and OM respiration rate, among other factors, but we note that Anderson et al (2015) observed this same threshold in a coral reef sand in Bermuda, to our knowledge the only other such published value. For ambient seawater ($\Omega_{arag} = 2.4$), reaching this dissolution threshold ($\Omega_{arag} = 1.75$) would require an addition of approximately 150 μmol kg^{-1} DIC from OM respiration. In our experiments, OM respiration during the first 1.8 h porewater residence time yielded between 100 and 160 μmol kg^{-1} DIC, suggesting that the dissolution threshold was reached by or shortly after 1.8 h. Indeed, the undersaturated columns did show positive net dissolution between 1.8 to 3.6 h. After this time, dissolution was relatively small for most columns, as respiration-driven dissolution became limited in the hypoxic porewater. Thus, in current, oversaturated seawater conditions, a minimum porewater residence time on the scale of 1.8 h (depending on respiration rates) is required before net dissolution occurs. This delay would presumably be longer in winter when respiration rates are lower. As ocean acidification progresses and the saturation state of overlying water moves closer to the critical Ω, however, this lag time will decrease, resulting in a faster onset of $CaCO_3$ dissolution. Ocean acidification is not expected to affect OM respiration rates, but warming is expected to do so, which could further expedite the onset of $CaCO_3$ dissolution (Hancke and Glud, 2004; Fink et al., 2017; Rassmann et al., 2018; Simone et al., 2021).

4.3. $CaCO_3$ dissolution occurs at bulk porewater Ω > 1

$CaCO_3$ dissolution that occurs at porewater $\Omega_{arag} > 1$ is typically attributed to dissolution of more soluble forms of $CaCO_3$ (e.g., high-Mg calcite), based on the assumption that any given $CaCO_3$ species will not dissolve prior to thermodynamic undersaturation of bulk porewater (Andersson, 2015). However, both our aragonite and calcite ^{13}C spike experiments showed clearly that dissolution can occur at porewater $\Omega > 1$ (Fig. 5). The aragonite spike experiment had significant dissolution at $\Omega_{arag} > 1$ by 1.8 h in the high-Ω treatment (Fig. 5A), and the calcite spike experiment showed dissolution at $\Omega_{calc} > 1$ in both the high- and low-Ω treatments, even though porewater remained oversaturated for the entirety of the experiments (Fig. 5B). Calcite dissolution was apparent at $1.3 < \Omega_{calc} < 2.2$, in alignment with the critical dissolution threshold $\Omega = 1.75$ suggested in Fig. 4. Such dissolution in supersaturated porewater may occur in acidic microniches, caused by either microbial activity embedded within highly porous, biogenic carbonate, or by locally-

accumulated CO_2 in high tortuosity flow paths (Freiwald, 1995; Kessler et al., 2014). In our case, using abiotic $CaCO_3$ with low intragranular porosity, the latter is most likely responsible. Although high-Mg calcite may indeed play a role in higher than expected dissolution threshold Ω's, especially in coastal areas where more soluble $CaCO_3$ species are common (Lowenstam, 1954; Compere and Bates, 1973; McClintock et al., 2011; Lebrato et al., 2016), our results suggest that less soluble $CaCO_3$ morphologies can dissolve well before measured porewater Ω becomes undersaturated, and thus may also contribute to seawater acid titration at higher saturation states.

4.4. $CaCO_3$ dissolution significantly increases in near-future ocean acidification conditions

At all porewater residence times considered, cumulative $CaCO_3$ dissolution increased as inlet Ω decreased. For current seawater saturation ($\Omega_{arag} = 2.4$), dissolution averaged 24.5 ± 23.8 mmol m^{-2} d^{-1} after 5.4 h porewater residence time. As a rough estimate for in situ rates, we divide this value by two—to account for the fact that our experiment's unidirectional flow of seawater *out of* sediment requires an approximate equal surface area for flow *into* sediment—yielding 12.3 ± 11.9 mmol m^{-2} d^{-1}. With acidification, this rate increased by 25.6 mmol CaCO3 m^{-2} d^{-1}, per unit Ω_{arag} decrease (for 5.4-h residence time). As an estimate for in situ conditions—again, dividing the value by two to account for inflow and outflow—the response is approximately 12.8 mmol CaCO3 m^{-2} d^{-1}, per unit Ω_{arag} decrease. In the California Current system, water column Ω_{arag} is projected to be consistently below 1.5, and bottom water below 1.0 by 2050 (Gruber et al., 2012). Considering these projections, and our 5.4-h residence time regression, benthic $CaCO_3$ dissolution could more than double by mid-century. Although our study is for nighttime rates, photosynthesis in sandy sediments does not appear to change with ocean acidification (although data suggests it may increase in cohesive sediments) (Fink et al., 2017; Vopel et al., 2018; Simone et al., 2021); thus considering daytime processes should not alter the slope of the dissolution:Ω_{arag} relationship. Hence, our observed slope may be a reasonable estimate for the benthic response to ocean acidification in photic areas as well. An important consideration for applying this rate to future acidification, however, is whether or not the delivery of $CaCO_3$ to shelf sands will keep pace with increased dissolution.

4.5. Similarity between carbonate-poor and carbonate-rich sands

Both the current rate of $CaCO_3$ dissolution, and response to acidification in our low-carbonate sand are similar to measurements in high-carbonate sands from coral reefs. Our sediment area-normalized rate—12.3 ± 11.9 mm ol m^{-2} d^{-1} for current seawater Ω (5.4 h porewater residence time)—falls within the range of nighttime rates measured in coral reef sands, typically between 7 and 24 mmol m^{-2} d^{-1} (Andersson et al., 2007; Rao et al., 2012; Cyronak et al., 2013a; Cyronak et al., 2013b; Cyronak and Eyre, 2016; Stoltenberg et al., 2020). However, global estimates for the carbonate-poor shelf typically assume dissolution rates more than an order of magnitude lower than this (Milliman, 1993; Krumins et al., 2013; O'Mara and Dunne, 2019). Furthermore, a comprehensive study of alkalinity release from sandy shelf sediments in the North Sea estimated average $CaCO_3$ dissolution at 2.7 mmol m^{-2} d^{-1} (Brenner et al., 2016). Thus, it is possible that our dissolution rates, measured over a relatively long porewater residence time, are too high, and that shorter porewater residence times may better reflect in situ conditions (Fig. 4). However, our dissolution rate for 5.4 h porewater residence time matches well with the average $CaCO_3$ production rate (equivalent to 11 mmol m^{-2} d^{-1}) for the California shelf, and thus may be reasonable for our field site and similar near-shore, carbonate-poor sands with little $CaCO_3$ accumulation (Smith, 1972).

The response of our sand to acidification was relatively consistent across porewater residence times (-11.5 to −13.7 mmol $CaCO_3$ dissolution m^{-2} d^{-1}, per unit Ω_{arag}), and was also similar to that measured in high-carbonate sands. Benthic chamber studies in coral reefs have measured acidification responses between −7.7 mmol CaCO3 m^{-2} d^{-1}, per unit Ω_{arag} for nighttime rates (Cyronak and Eyre, 2016), and −11.5 mmol CaCO3 m^{-2} d^{-1}, per unit Ω_{arag} for a daily average across five reef ecosystems (Eyre et al., 2018). Furthermore, the point at which sands transition from net precipitating to net dissolving was also similar between sand types. For a short residence time, our transition point approached the critical porewater dissolution threshold, $\Omega_{arag} = 1.75$, while at longer residence times, our sand was already net dissolving at current seawater saturation ($\Omega_{arag} = 2.4$) (Fig. 4). Extrapolating the linear model for 5.4-h porewater residence time, however, yields a "transition point" of $\Omega_{arag} = 3.1$, which is similar to measurements in coral reef sands, between $\Omega_{arag} = 2.9$ to 3.0 (Cyronak and Eyre, 2016; Eyre et al., 2018). Kessler et al (2020) found a lower transition point, around $\Omega_{arag} = 2.2$ using short FTR's (1.2 cm height) with high-carbonate, but this is likely due to a shorter porewater residence time. Many coral reef environments have yet to reach this transition threshold, but our site has naturally lower Ω and thus—given sufficient in situ porewater residence time—is likely already net dissolving. Because dissolution rates vary not only with Ω but also with porewater residence time, this transition point is also sensitive to changing porewater advection conditions (as driven by e.g., changing wind and current patterns).

The similar dissolution rates and responses to acidification in high- and low-carbonate sands, despite the vast difference in $CaCO_3$ content—i.e., <1% in our sand vs. nearly 100% in coral reef sands—suggest that the small amount of $CaCO_3$ in our sand was not a significant limit on dissolution, at least on the timescale of our experiments. Instead, factors related to porewater acidity, including Ω of the overlying water, and O_2 and OM available for aerobic respiration (and subsequent production of CO_2) are more important drivers of dissolution (Higgins et al., 2009). In other words, our carbonate-poor sand behaves much like carbonate-replete sands, in that they are acid (CO_2)-

limited rather than base ($CaCO_3$)-limited. An acidifying ocean will deliver more acid to these sediments, and thus directly increase dissolution, as long as $CaCO_3$ does not become limiting. Given our measured dissolution rates for current seawater conditions, the mass of $CaCO_3$ in our column volume would last approximately 1 year for a 5.4-h porewater residence time, or longer for shorter residence times. With continued acidification, it is thus possible that the available $CaCO_3$ base could be exhausted, depending on porewater residence time and rate of replenishment by sedimentation.

4.6. Carbonate-poor shelf sands may transition from net source of acid to net source of buffering

If $CaCO_3$ does not become limiting, increased dissolution could fundamentally change the sediment's net impact on overlying water column chemistry. The ratio of benthic alkalinity production to DIC production (ΔAlk:ΔDIC, i.e., the flux ratio) is a useful metric for quantifying the effect of sediment processes on water column Ω and pH (see Middelburg et al., 2020 for detailed explanation). ΔAlk:ΔDIC values < 1 imply net production of CO_2, which lowers seawater pH and Ω, whereas values > 1 imply net production of CO_3^{2-}, which increases pH and Ω. In the present ocean, the carbonate-poor sands in our study have ΔAlk:ΔDIC well below 1 across all measured porewater residence times (Fig. 8). Although $CaCO_3$ dissolution does occur after 1.8 h, it produces insufficient alkalinity to negate the CO_2 produced by aerobic respiration. As ocean acidification decreases seawater Ω, however, $CaCO_3$ dissolution increases to the point at which production of dissolution-derived CO_3^{2-}, along with alkalinity from anaerobic respiration, exceeds the production of CO_2. At that point, ΔAlk:ΔDIC > 1, and the net effect on overlying water is buffering, instead of acidifying.

The point at which this transition occurs depends on porewater residence time, since longer residence times allow for more $CaCO_3$ dissolution and anaerobic respiration, while aerobic OM respiration rates fall as porewater O_2 is depleted. In our study, the sand transitioned to net buffering when inlet water Ω_{arag} = 0.96 and 0.69 (Ω_{calc} = 1.50 and 1.07), for 1.8-h to 5.4-h porewater residence times, respectively. Longer porewater residence times would likely yield transition points at even higher Ω. While the mean global ocean is expected to remain oversaturated with respect to aragonite over the next century, areas with naturally acidic water, including the Arctic and upwelled water along the California coast, are expected to fall well below Ω_{arag} < 1, and indeed in some areas already have (Steinacher et al., 2009; Gruber et al., 2012; Feely et al., 2018). Thus, permeable shelf sediments in these areas may cross the ΔAlk:ΔDIC > 1 threshold this century, at which point they become a buffer to water column acidification, given sufficient stock or input of $CaCO_3$. In this case, the effect of sediments on the overlying water fundamentally changes.

4.7. Low-carbonate sands and ocean acidification: global considerations

Given its large global area, the carbonate-poor shelf may be an important component of the ocean $CaCO_3$ cycle. For example, data suggest that seawater overlying the continental shelves has recently transitioned from a net source to net sink of atmospheric CO_2 (Andersson and Mackenzie, 2004; Andersson et al., 2005; Mackenzie et al., 2005; Laruelle et al., 2018). While this is largely attributed to changes in both the physical and biological pump, the contribution of increased $CaCO_3$ dissolution in shelf sediments remains poorly quantified. Because our experiments impose a constant porewater residence time and cannot account for

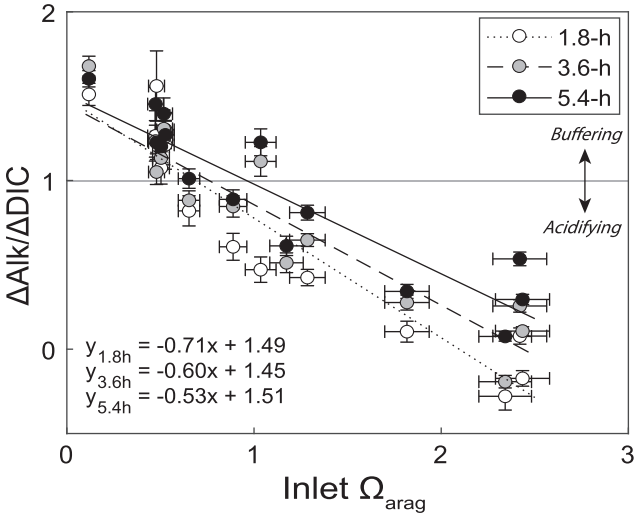

Fig. 8. Ratio of alkalinity to DIC production (ΔAlk:ΔDIC) as a function of Ω_{inlet}. Linear relationships are shown for all three porewater residence times: r^2 = 0.88, 0.87, and 0.83 for 1.8-, 3.6-, and 5.4-h porewater residence time, respectively, and $p < 0.001$ for all three. The sand transitions from acidifying to buffering between $\Omega_{aragonite}$ = 0.69 and 0.96, depending on porewater residence time. (Linear fits exclude data for the inlet $\Omega_{aragonite}$ = 0.1 experiment.).

spatial and temporal heterogeneity, we do not attempt to extrapolate absolute, measured dissolution rates to the entire low-carbonate shelf; constraining absolute rates will require more in situ data from a range of environments and advective conditions. Regardless of the absolute dissolution rate currently, however, our data clearly show that total dissolution on the low-carbonate shelf may increase significantly as the ocean becomes more acidic (Fig. 4). Our results suggest that a decrease in Ω_{arag} of 0.5 units (e.g., to $\Omega_{arag} = 1.9$ at our site)—which is expected for surface water by 2100 (Caldeira and Wickett, 2005; Gruber et al., 2012)–would increase current dissolution rates by approximately 12 mmol m^{-2} d^{-1} (consistent across all porewater residence times tested). Extrapolating this to the global low-carbonate shelf area ($1.5*10^7$ km^2; Milliman, 1993) yields a dissolution *increase* of 0.79 Gt C y^{-1}, or for only the area below the effective photic zone, 0.53 Gt C y^{-1}, which is more than an order of magnitude higher than the estimated total $CaCO_3$ production for the low-carbonate shelf area (Milliman, 1993; Iglesias-Rodriguez et al., 2002; Krumins et al., 2013). This projected increase may be unreasonably high if actual in situ advection rates are beyond the bounds (in particular, shorter) of those tested here. Alternatively, this may imply that increased dissolution in sediments may exhaust annual $CaCO_3$ production.

By definition, the carbonate-poor shelf has little to no $CaCO_3$ accumulation. Milliman (1993) estimated that an average of 25% of $CaCO_3$ produced in this zone accumulates, but other authors have estimated accumulation closer to zero (O'Mara and Dunne, 2019). A small $CaCO_3$ surplus could fuel all, or a fraction of the enhanced dissolution anticipated with ocean acidification. However, in areas that currently have no $CaCO_3$ accumulation, sediments are already $CaCO_3$-limited, and dissolution therefore cannot increase at all. Thus, the annual production of $CaCO_3$ in much of the shelf may be insufficient to support the potential dissolution enhancement, and benthic $CaCO_3$ could be exhausted. If this occurs, ΔAlk:ΔDIC would remain below 1 and the $CaCO_3$-poor shelf would continue to be a source of acid to the overlying water column.

The potential for carbonate-poor sands to support enhanced dissolution with ocean acidification thus likely relies on consumption of legacy $CaCO_3$, and/or delivery of allochthonous $CaCO_3$ to the sediment. A variety of global change processes could contribute to both. For example, legacy $CaCO_3$ already present in continental shelf sands may be increasingly exposed to acidifying seawater by increased turbulence from storm activity, and/or deeper porewater advection from increased bottom water current speeds (Hu et al., 2020). Similarly, changes in wave climate, sea level rise, increased storm activity, precipitation and river discharge all conspire to increase erosion, especially along sandy coastlines (Ranasinghe, 2016; Vousdoukas et al., 2020). Currently, a quarter of the world's sandy beaches are eroding at > 0.5 m y^{-1} (Luijendijk et al., 2018). In areas with carbonate lithologies, such erosion could deliver $CaCO_3$ from land to coastal sediments, feeding enhanced dissolution rates. Alternatively, a reduction in $CaCO_3$ deposition (i.e., from acidification-related impacts on calcifier physiology) could limit benthic $CaCO_3$ dissolution and/or accumulation (Simeone et al., 2018). If carbonate-poor sands do become $CaCO_3$-limited as ocean acidification progresses, addition of $CaCO_3$ or other basic minerals to the shelf or coastal zone via "enhanced weathering" efforts could be considered as a tool to produce ocean alkalinity and sequester dissolved CO_2 via the anticipated increase in dissolution (Harvey, 2008; Ilyina et al., 2013; Meysman and Montserrat, 2017).

5. SUMMARY

Our study provides clear evidence that $CaCO_3$ dissolution in carbonate-poor sands a) occurs prior to undersaturation of the overlying water; b) increases as seawater Ω decreases; and c) increases with porewater residence time. In current seawater conditions, net dissolution occurred after 1.8 h porewater residence time as a result of aerobic OM respiration decreasing porewater Ω. Dissolution occurred sooner, and at higher rates, in lower-Ω treatments.

The sand in our study is currently a source of acid to the overlying water (i.e., ΔAlk/ΔDIC < 1), but may transition to a net buffer (ΔAlk/ΔDIC > 1) between $\Omega_{arag} = 0.69$ and 0.96 ($\Omega_{calc} = 1.07$ and 1.50), depending on porewater residence time. The higher end of this threshold will be reached in many parts of the ocean with naturally acidic water, including the California Current, by the middle of this century, so sediments could fundamentally transition to a net water column buffer, provided sufficient $CaCO_3$ substrate.

Compared to carbonate-rich, coral reef sands, the carbonate-poor sand in our study had similar rates of $CaCO_3$ dissolution, and responds similarly to decreasing seawater Ω. The slope of the $CaCO_3$ dissolution vs water column Ω regression in our study is similar to those from coral reef sands, suggesting that carbonate-poor sands have the potential to respond similarly to ocean acidification. A key question for future study is whether or not the pool of existing $CaCO_3$ in carbonate-poor sands is sufficient to support increased dissolution. Global change processes such as higher storm frequency and enhanced erosion, or even intentional delivery of $CaCO_3$ to the coastal zone may increase the availability of $CaCO_3$ to support enhanced dissolution.

Declaration of Competing Interest

The authors declare that they have no known competing financial interests or personal relationships that could have appeared to influence the work reported in this paper.

ACKNOWLEDGEMENTS

This research was supported by the USC Department of Earth Sciences, the Wrigley Institute for Environmental Studies, and the Victoria J. Bertics Graduate Fellowship. The authors would like to acknowledge Nick Rollins for assistance with technical and analytical issues; Jaclyn Pittman, Liana Kaye-Lew and Rabia Ghulam-Ali for help collecting and analyzing samples; Aaron Celestian for help with mineralogy analysis; and Doug Hammond, Jess Adkins and Josh West for helpful discussions. We are also grateful

to Filip Meysman, Andreas Andersson, and two anonymous reviewers for their constructive feedback during the review process.

APPENDIX A. SUPPLEMENTARY MATERIAL

Supplementary data to this article can be found online at https://doi.org/10.1016/j.gca.2022.04.031.

REFERENCES

Amos C. M., Castelao R. M. and Medeiros P. M. (2019) Offshore transport of particulate organic carbon in the California Current System by mesoscale eddies. *Nat. Commun.* **10**, 1–8.

Andersson A. J. (2015) A fundamental paradigm for coral reef carbonate sediment dissolution. *Front. Mar. Sci.* **2**, 52.

Andersson A. J., Bates N. R. and Mackenzie F. T. (2007) Dissolution of carbonate sediments under rising pCO 2 and ocean acidification: observations from Devil's Hole, Bermuda. *Aquat. Geochem.* **13**, 237–264.

Andersson A. J. and Gledhill D. (2013) Ocean acidification and coral reefs: effects on breakdown, dissolution, and net ecosystem calcification. *Ann. Rev. Mar. Sci.* **5**, 321–348.

Andersson A. J. and Mackenzie F. T. (2012) Revisiting four scientific debates in ocean acidification research. *Biogeosciences* **9**, 893–905.

Andersson A. J. and Mackenzie F. T. (2004) Shallow-water oceans: a source or sink of atmospheric CO2? *Front. Ecol. Environ.* **2**, 348–353.

Andersson A. J., MacKenzie F. T. and Lerman A. (2005) Coastal ocean and carbonate systems in the high CO2 world of the anthropocene. *Am. J. Sci.* **305**, 875–918.

Boucher G., Clavier J., Hily C. and Gattuso J.-P. (1998) Contribution of soft-bottoms to the community metabolism (primary production and calcification) of a barrier reef flat (Moorea, French Polynesia). *J. Exp. Mar. Bio. Ecol.* **225**, 269–283.

Boudreau B. P., Huettel M., Forster S., Jahnke R., McLachlan A., Middelburg J. J., Nielsen P., Sansone F., Taghon G. and Van Raaphorst W. (2001) Permeable marine sediments: overturning an old paradigm. *EOS. Trans. Am. Geophys. Union* **82**, 133–136.

Bourke M. F., Marriott P. J., Glud R. N., Hasler-Sheetal H., Kamalanathan M., Beardall J., Greening C. and Cook P. L. M. (2017) Metabolism in anoxic permeable sediments is dominated by eukaryotic dark fermentation. *Nat. Geosci.* **10**, 30–35.

Brenner H., Braeckman U., Le Guitton M. and Meysman F. J. R. (2016) The impact of sedimentary alkalinity release on the water column CO2system in the North Sea. *Biogeosciences* **13**, 841–863.

Broecker W. S. and Peng T. (1987) The role of CaCO3 compensation in the glacial to interglacial atmospheric CO2 change. *Global Biogeochem. Cycles* **1**, 15–29.

Bühring S. I., Ehrenhauss S., Kamp A., Moodley L. and Witte U. (2006) Enhanced benthic activity in sandy sublittoral sediments: evidence from 13C tracer experiments. *Mar. Biol. Res.* **2**, 120–129.

Cai W. J. (2011) Estuarine and coastal ocean carbon paradox: CO2 sinks or sites of terrestrial carbon incineration? *Ann. Rev. Mar. Sci.* **3**, 123–145.

Caldeira, K., Wickett, M.E., 2005. Ocean model predictions of chemistry changes from carbon dioxide emissions to the atmosphere and ocean. J. Geophys. Res. Ocean. **110**.

Chisholm J. R. M. and Gattuso J. (1991) Validation of the alkalinity anomaly technique for investigating calcification of photosynthesis in coral reef communities. *Limnol. Oceanogr.* **36**, 1232–1239.

Compere, Jr, E. L. and Bates J. M. (1973) Determination of calcite: aragonite ratios in mollusc shells by infrared spectra 1. *Limnol. Oceanogr.* **18**, 326–331.

Cyronak T. and Eyre B. D. (2016) The synergistic effects of ocean acidification and organic metabolism on calcium carbonate (CaCO3) dissolution in coral reef sediments. *Mar. Chem.* **183**, 1–12.

Cyronak T., Santos I. R. and Eyre B. D. (2013a) Permeable coral reef sediment dissolution driven by elevated pCO2 and pore water advection. *Geophys. Res. Lett.* **40**, 4876–4881.

Cyronak T., Santos I. R., McMahon A. and Eyre B. D. (2013b) Carbon cycling hysteresis in permeable carbonate sands over a diel cycle: Implications for ocean acidification. *Limnol. Oceanogr.* **58**, 131–143.

Dong S., Berelson W. M., Rollins N. E., Subhas A. V, Naviaux J. D., Celestian A. J., Liu X., Turaga N., Kemnitz N. J. and Byrne R. H. (2019) Aragonite dissolution kinetics and calcite/aragonite ratios in sinking and suspended particles in the North Pacific. *Earth Planet. Sci. Lett.* **515**, 1–12.

Emerson S. and Bender M. L. (1981) Carbon fluxes at the sediment-water interface: Calcium carbonate preservation. *J. Mar. Res.* **39**, 139–162.

Emery K. O. (1968) Relict sediments on continental shelves of world. *Am. Assoc. Pet. Geol. Bull.* **52**, 445–464.

Eyre B. D., Andersson A. J. and Cyronak T. (2014) Benthic coral reef calcium carbonate dissolution in an acidifying ocean. *Nat. Clim. Chang.* **4**, 969.

Eyre B. D., Cyronak T., Drupp P., De Carlo E. H., Sachs J. P. and Andersson A. J. (2018) Coral reefs will transition to net dissolving before end of century. *Science* **359**, 908–911.

Feely R. A., Okazaki R. R., Cai W.-J., Bednaršek N., Alin S. R., Byrne R. H. and Fassbender A. (2018) The combined effects of acidification and hypoxia on pH and aragonite saturation in the coastal waters of the California current ecosystem and the northern Gulf of Mexico. *Cont. Shelf Res.* **152**, 50–60.

Fink A., den Haan J., Chennu A., Uthicke S. and de Beer D. (2017) Ocean Acidification Changes Abiotic Processes but Not Biotic Processes in Coral Reef Sediments. *Front. Mar. Sci.* **4**, 73.

Franke U., Polerecky L., Precht E. and Huettel M. (2006) Wave tank study of particulate organic matter degradation in permeable sediments. *Limnol. Oceanogr.* **51**, 1084–1096.

Freiwald A. (1995) Bacteria-induced carbonate degradation: a taphonomic case study of Cibicides lobatulus from a high-boreal carbonate setting. *Palaios*, 337–346.

Friedlingstein P., O'Sullivan M., Jones M. W., Andrew R. M., Hauck J., Olsen A., Peters G. P., Peters W., Pongratz J. and Sitch S. (2020) Global carbon budget 2020. *Earth Syst. Sci. Data* **12**, 3269–3340.

Gattuso J.-P., Frankignoulle M. and Wollast R. (1998) Carbon and carbonate metabolism in coastal aquatic ecosystems. *Annu. Rev. Ecol. Syst.* **29**, 405–434.

Gattuso J.-P., Gentili B., Duarte C. M., Kleypas J. A., Middelburg J. J. and Antoine D. (2006) Light availability in the coastal ocean: impact on the distribution of benthic photosynthetic organisms and their contribution to primary production. *Biogeosciences*.

Gruber N., Hauri C., Lachkar Z., Loher D., Frölicher T. L. and Plattner G.-K. (2012) Rapid progression of ocean acidification in the California Current System. *Science* **337**, 220–223.

Hall S. J. (2002) The continental shelf benthic ecosystem: current status, agents for change and future prospects. *Environ. Conserv.* **29**, 350–374.

Hancke K. and Glud R. N. (2004) Temperature effects on respiration and photosynthesis in three diatom-dominated benthic communities. *Aquat. Microb. Ecol.* **37**, 265–281.

Harvey L. D. D. (2008) *Mitigating the atmospheric CO2 increase and ocean acidification by adding limestone powder to upwelling regions*. J. Geophys. Res, Ocean, p. 113.

Hayes M. O. (1967) Relationship between coastal climate and bottom sediment type on the inner continental shelf. *Mar. Geol.* **5**, 111–132.

van Heuven S., Pierrot D., Rae J. W. B., Lewis E. and Wallace D. W. R. (2011) MATLAB Program Developed for CO2 System Calculations. ORNL/CDIAC-105b. Available at: https://doi.org/10.3334/CDIAC/otg.CO2SYS_MATLAB_v1.1.

Higgins J. A., Fischer W. W. and Schrag D. P. (2009) Oxygenation of the ocean and sediments: consequences for the seafloor carbonate factory. *Earth Planet. Sci. Lett.* **284**, 25–33.

Hu S., Sprintall J., Guan C., McPhaden M. J., Wang F., Hu D. and Cai W. (2020) Deep-reaching acceleration of global mean ocean circulation over the past two decades. *Sci. Adv.* **6**.

Huettel M., Berg P. and Kostka J. E. (2014) Benthic Exchange and Biogeochemical Cycling in Permeable Sediments. *Ann. Rev. Mar. Sci.* **6**, 23–51.

Iglesias-Rodriguez M. D., Armstrong R., Feely R., Hood R., Kleypas J., Milliman J. D., Sabine C. and Sarmiento J. (2002) Progress made in study of ocean's calcium carbonate budget. *Eos. Trans. Am. Geophys. Union* **83**, 365–375.

Ilyina T., Wolf-Gladrow D., Munhoven G. and Heinze C. (2013) Assessing the potential of calcium-based artificial ocean alkalinization to mitigate rising atmospheric CO2 and ocean acidification. *Geophys. Res. Lett.* **40**, 5909–5914.

Jahnke R. A., Craven D. B. and Gaillard J.-F. (1994) The influence of organic matter diagenesis on CaCO3 dissolution at the deep-sea floor. *Geochim. Cosmochim. Acta* **58**, 2799–2809.

Jenkins C. (2021) *dbSEABED*. INSTAAR, Univ, Color. Boulder. Available at: http://instaar.colorado.edu/~jenkinsc/dbseabed/.

Kessler A. J., Cardenas M. B., Santos I. R. and Cook P. L. M. (2014) Enhancement of denitrification in permeable carbonate sediment due to intra-granular porosity: A multi-scale modelling analysis. *Geochim. Cosmochim. Acta* **141**, 440–453.

Kessler A. J., Chen Y.-J., Waite D. W., Hutchinson T., Koh S., Popa M. E., Beardall J., Hugenholtz P., Cook P. L. M. and Greening C. (2019) Bacterial fermentation and respiration processes are uncoupled in anoxic permeable sediments. *Nat. Microbiol.* **4**, 1014.

Kessler A. J., Rogers A., Cyronak T., Bourke M. F., Hasler-Sheetal H., Glud R. N., Greening C., Meysman F. J. R., Eyre B. D. and Cook P. L. M. (2020) Pore water conditions driving calcium carbonate dissolution in reef sands. *Geochim. Cosmochim. Acta* **279**, 16–28.

Krumins V., Gehlen M., Arndt S., Van Cappellen P. and Regnier P. (2013) Dissolved inorganic carbon and alkalinity fluxes from coastal marine sediments: Model estimates for different shelf environments and sensitivity to global change. *Biogeosciences* **10**, 371–398.

Lantz C. A., Carpenter R. C. and Edmunds P. J. (2017a) Calcium carbonate (CaCO3) sediment dissolution under elevated concentrations of carbon dioxide (CO2) and nitrate (NO3−). *J. Exp. Mar. Bio. Ecol.* **495**, 48–56.

Lantz C. A., Schulz K. G. and Eyre B. D. (2020) Ocean Acidification and Short-Term Organic Matter Enrichment Alter Coral Reef Sediment Metabolism Through Different Pathways. *J. Geophys. Res. Biogeosciences* **125**.

Lantz C. A., Schulz K. G., Stoltenberg L. and Eyre B. D. (2017b) The short-term combined effects of temperature and organic matter enrichment on permeable coral reef carbonate sediment metabolism and dissolution. *Biogeosciences* **14**, 5377–5391.

Laruelle G. G., Cai W.-J., Hu X., Gruber N., Mackenzie F. T. and Regnier P. (2018) Continental shelves as a variable but increasing global sink for atmospheric carbon dioxide. *Nat. Commun.* **9**, 454.

Lebrato M., Andersson A. J., Ries J. B., Aronson R. B., Lamare M. D., Koeve W., Oschlies A., Iglesias-Rodriguez M. D., Thatje S. and Amsler M. (2016) Benthic marine calcifiers coexist with CaCO3-undersaturated seawater worldwide. *Global Biogeochem. Cycles* **30**, 1038–1053.

Lewis E. and Wallace D. W. R. (1998) Program Developed for CO2 System Calculations, ORNL/CDIAC-105. Available at: https://salish-sea.pnnl.gov/media/ORNL-CDIAC-105.pdf.

Lowenstam H. A. (1954) Factors affecting the aragonite: calcite ratios in carbonate-secreting marine organisms. *J. Geol.* **62**, 284–322.

Luijendijk A., Hagenaars G., Ranasinghe R., Baart F., Donchyts G. and Aarninkhof S. (2018) The state of the world's beaches. *Sci. Rep.* **8**, 6641.

Mackenzie F. T., Andersson A., Lerman A. and Ver L. M. (2005) Boundary exchanges in the global coastal margin: implications for the organic and inorganic carbon cycles. In *The Sea, Volume 13: The Global Coastal Ocean* (ed. A. R. R. and K. H. Brink). Harvard University Press, Cambridge, MA. pp. 193–225.

McClintock J. B., Amsler M. O., Angus R. A., Challener R. C., Schram J. B., Amsler C. D., Mah C. L., Cuce J. and Baker B. J. (2011) The Mg-calcite composition of Antarctic echinoderms: Important implications for predicting the impacts of ocean acidification. *J. Geol.* **119**, 457–466.

McGinnis D. F., Sommer S., Lorke A., Glud R. N. and Linke P. (2014) Quantifying tidally driven benthic oxygen exchange across permeable sediments: An aquatic eddy correlation study. *J. Geophys. Res. Ocean.* **119**, 6918–6932.

McLachlan A. (1989) Water filtration by dissipative beaches. *Limnol. Oceanogr.* **34**, 774–780.

Megens L., Van der Plicht J. and De Leeuw J. W. (2001) Temporal variations in 13C and 14C concentrations in particulate organic matter from the southern North Sea. *Geochim. Cosmochim. Acta* **65**, 2899–2911.

Meysman F. J. R. and Montserrat F. (2017) Negative CO2 emissions via enhanced silicate weathering in coastal environments. *Biol. Lett.* **13**, 20160905.

Middelburg J. J., Soetaert K. and Hagens M. (2020) Ocean alkalinity, buffering and biogeochemical processes. *Rev. Geophys.* **58**.

Milliman J. (1993) Production and accumulation of calcium carbonate in the Ocean: Budget of a non-steady state. *Global Biogeochem. Cycles* **7**, 927–957.

Milliman J. and Droxler A. (1996) Neritic and pelagic carbonate sedimentation in the marine environment: ignorance is not bliss. *Geol. Rundschau* **85**, 496–504.

Moore W. S., Sarmiento J. L. and Key R. M. (2008) Submarine groundwater discharge revealed by 228 Ra distribution in the upper Atlantic Ocean. *Nat. Geosci.* **1**, 309–311.

Moreno A. R., Garcia C. A., Larkin A. A., Lee J. A., Wang W.-L., Moore J. K., Primeau F. W. and Martiny A. C. (2020) Latitudinal gradient in the respiration quotient and the implications for ocean oxygen availability. *Proc. Natl. Acad. Sci.* **117**, 22866–22872.

Morse J. W. (1985) Chemistry of calcium carbonate-rich shallow water sediments in the Bahamas. *Am. J. Sci.* **285**, 147–185.

Naviaux J. D., Subhas A. V, Rollins N. E., Dong S., Berelson W. M. and Adkins J. F. (2019) Temperature dependence of calcite dissolution kinetics in seawater. *Geochim. Cosmochim. Acta* **246**, 363–384.

Nickl H. J. and Henisch H. K. (1969) Growth of calcite crystals in gels. *J. Electrochem. Soc.* **116**, 1258–1260.

O'Mara N. A. and Dunne J. P. (2019) Hot spots of carbon and alkalinity cycling in the coastal oceans. *Sci. Rep.* **9**, 1–8.

Oberdorfer J. A. and Buddemeier and R. W. (1986) Coral-reef hydrology: field studies of water movement within a barrier reef. *Coral Reefs* **5**, 7–12.

Orr J. C., Epitalon J. M., Dickson A. G. and Gattuso J. P. (2018) Routine uncertainty propagation for the marine carbon dioxide system. *Mar. Chem.* **207**, 84–107.

Perez F. F., Fontela M., García-Ibáñez M. I., Mercier H., Velo A., Lherminier P., Zunino P., De La Paz M., Alonso-Pérez F. and Guallart E. F. (2018) Meridional overturning circulation conveys fast acidification to the deep Atlantic Ocean. *Nature* **554**, 515–518.

Precht E. and Huettel M. (2003) Advective pore-water exchange driven by surface gravity waves and its ecological implications. *Limnol. Oceanogr.* **48**, 1674–1684.

Precht E. and Huettel M. (2004) Rapid wave-driven advective pore water exchange in a permeable coastal sediment. *J. Sea Res.* **51**, 93–107.

Ranasinghe R. (2016) Assessing climate change impacts on open sandy coasts: A review. *Earth-science Rev.* **160**, 320–332.

Rao A. M. F., Polerecky L., Ionescu D., Meysman F. J. R. and De Beer D. (2012) The influence of pore-water advection, benthic photosynthesis, and respiration on calcium carbonate dynamics in reef sands. *Limnol. Oceanogr.* **57**, 809–825.

Rassmann J., Lansard B., Gazeau F., Guidi-Guilvard L., Pozzato L., Alliouane S., Grenz C. and Rabouille C. (2018) Impact of ocean acidification on the biogeochemistry and meiofaunal assemblage of carbonate-rich sediments: Results from core incubations (Bay of Villefranche, NW Mediterranean Sea). *Mar. Chem.* **203**, 102–119.

Reimers C. E., Stecher, III, H. A., Taghon G. L., Fuller C. M., Huettel M., Rusch A., Ryckelynck N. and Wild C. (2004) In situ measurements of advective solute transport in permeable shelf sands. *Cont. Shelf Res.* **24**, 183–201.

Riedl R. J., Huang N. and Machan R. (1972) The subtidal pump: a mechanism of interstitial water exchange by wave action. *Mar. Biol.* **13**, 210–221.

Rusch A., Huettel M., Wild C. and Reimers C. E. (2006) Benthic oxygen consumption and organic matter turnover in organic-poor, permeable shelf sands. *Aquat. Geochemistry* **12**, 1–19.

Santos I. R., Eyre B. and Huettel M. (2012) The driving forces of porewater and groundwater flow in permeable coastal sediments : A review. *Estuar. Coast. Shelf Sci.* **98**, 1–15.

Shum K. T. and Sundby B. (1996) Organic matter processing in continental shelf sediments—the subtidal pump revisited. *Mar. Chem.* **53**, 81–87.

Simeone S., Molinaroli E., Conforti A. and De Falco G. (2018) Impact of ocean acidification on the carbonate sediment budget of a temperate mixed beach. *Clim. Change* **150**, 227–242.

Simone M. N., Schulz K. G., Eyre B. D. and Oakes J. M. (2021) Ocean acidification may mitigate negative effects of warming on carbon burial potential in subtidal unvegetated estuarine sediments. *Limnol. Oceanogr.* **66**, 2953–2966.

Smith S. V. (1972) Production of calcium carbonate on the mainland shelf of Southern California. *Limnol. Oceanogr.* **17**, 28–41.

Steinacher M., Joos F., Frölicher T. L., Plattner G.-K. and Doney S. C. (2009) Imminent ocean acidification in the Arctic projected with the NCAR global coupled carbon cycle-climate model. *Biogeosciences* **6**, 515–533.

Stoltenberg L., Schulz K. G., Cyronak T. and Eyre B. D. (2020) Seasonal variability of calcium carbonate precipitation and dissolution in shallow coral reef sediments. *Limnol. Oceanogr.* **65**, 876–891.

Stoltenberg L., Schulz K. G., Lantz C. A., Cyronak T. and Eyre B. D. (2021) Late Afternoon Seasonal Transition to Dissolution in a Coral Reef: An Early Warning of a Net Dissolving Ecosystem? *Geophys. Res. Lett.* **48**.

Subhas A. V., Adkins J. F., Rollins N. E., Naviaux J., Erez J. and Berelson W. M. (2017) Catalysis and chemical mechanisms of calcite dissolution in seawater. *Proc. Natl. Acad. Sci.* **114**, 8175–8180. Available at: http://www.pnas.org/lookup/doi/10.1073/pnas.1703604114.

Subhas A. V., Rollins N. E., Berelson W. M., Erez J., Ziveri P., Langer G. and Adkins J. F. (2018) The dissolution behavior of biogenic calcites in seawater and a possible role for magnesium and organic carbon. *Mar. Chem.* **205**, 100–112.

Sulpis O., Boudreau B. P., Mucci A., Jenkins C., Trossman D. S., Arbic B. K. and Key R. M. (2018) Current CaCO3 dissolution at the seafloor caused by anthropogenic CO2. *Proc. Natl. Acad. Sci.* **115**, 11700–11705.

Thomas H., Bozec Y., Elkalay K. and De Baar H. J. W. (2004) Enhanced Open Ocean Storage of CO2 from Shelf Sea Pumping. *Science* **304**, 1005–1008.

Trnovsky D., Stoltenberg L., Cyronak T. and Eyre B. D. (2016) Antagonistic effects of ocean acidification and rising sea surface temperature on the dissolution of coral reef carbonate sediments. *Front. Mar. Sci.* **3**, 211.

Tsunogai S., Watanabe S. and Sato T. (1999) Is there a "continental shelf pump" for the absorption of atmospheric CO2? *Tellus B Chem. Phys. Meteorol.* **51**, 701–712.

Vopel K., Del-Río C. and Pilditch C. A. (2018) Effects of CO 2 enrichment on benthic primary production and inorganic nitrogen fluxes in two coastal sediments. *Sci. Rep.* **8**, 1–15.

Vousdoukas M. I., Ranasinghe R., Mentaschi L., Plomaritis T. A., Athanasiou P., Luijendijk A. and Feyen L. (2020) Sandy coastlines under threat of erosion. *Nat. Clim. Chang.* **10**, 260–263.

Wild C., Rasheed M., Jantzen C., Cook P., Struck U., Huettel M. and Boetius A. (2005) Benthic metabolism and degradation of natural particulate organic matter in carbonate and silicate reef sands of the northern Red Sea. *Mar. Ecol. Prog. Ser.* **298**, 69–78.

Wolf-Gladrow D. A., Zeebe R. E., Klaas C., Körtzinger A. and Dickson A. G. (2007) Total alkalinity: The explicit conservative expression and its application to biogeochemical processes. *Mar. Chem.* **106**, 287–300.

Yates K. K. and Halley R. B. (2006) Diurnal variation in rates of calcification and carbonate sediment dissolution in Florida Bay. *Estuaries and Coasts* **29**, 24–39.

Yates K. K. and Halley R. B. (2003) Measuring coral reef community metabolism using new benthic chamber technology. *Coral reefs* **22**, 247–255.

Zeebe R. E. (2012) History of seawater carbonate chemistry, atmospheric CO2, and ocean acidification. *Annu. Rev. Earth Planet. Sci.* **40**, 141–165.

Zeebe R. E. and Westbroek P. (2003) A simple model for the CaCO3 saturation state of the ocean: The "Strangelove", the "Neritan", and the "Cretan" Ocean. *Geochem., Geophys. Geosyst.* **4**.

Associate editor: Filip Meysman